Biomimetic Active Control of Propulsor Noise Using Conducting Polymers

Daniel Opila[1], Peter Madden, and Bryan D. Schmid

Department of Mechanical Engineering
Massachusetts Institute of Technology
Cambridge, MA 02139

Abstract

The field of biomimetics seeks to distill biological principles from nature and implement them in engineering systems in an effort to improve various performance metrics. In this paper, a biology-based approach is used to address the problem of radiated propulsor noise in underwater vehicles using active control. This approach is one of "tail articulation" of a stator blade, which is carried out using a suitable strategy that effectively alters the flow field impinging on a rotor downstream and in turn changes the radiated noise characteristics of the rotor blades. This articulation is accomplished by attaching an actuator at the trailing edge of an upstream stator blade and modulating it using a control strategy. Two actuation methods are used to articulate the stator-tail: a conducting polymer actuator and a stepper motor. An encapsulated conducting polymer (CP) actuator based on polypyrrole is designed, fabricated, and tested for operation in water. This CP actuator is shown to alter the flow field in an open channel water tunnel. Flow measurements are also conducted using a motor controlled articulation to yield greater actuator authority, at a Reynolds number of 4000. Wake deficits are reduced up to 60% with trailing edge articulation, and the corresponding radiated noise from the propulsor is predicted to drop by 5-10 dB. Wake deficit reduction occurs most effectively with Strouhal numbers of 0.25 to 0.35, the range previously reported by others to be the operating regime of propulsion efficiency in swimming fish.

1. INTRODUCTION

Swimming and flying animals exhibit rapid hovering, maneuvering, and cruise characteristics that surpass man's best achievements to date. These animals have been studied in an attempt to replicate their remarkable maneuvering capability [1-7] in small underwater vehicles. However, these maneuvering capabilities make extensive use of unsteady hydrodynamics, which are not easily applicable to the conventional steady-state hydrodynamics on which most current engineering vehicles are built.

Noise production is a constant concern in some types of underwater vehicles, especially those for military applications. Direct radiation is a major source of this noise and comes from several sources, including fluctuating forces, fluctuating volumes, and turbulence [8]. The operation of a propulsor in a non-uniform wake causes fluctuating thrust and side forces. Specifically, a stator or guide vane produces a wake deficit in a uniform flow. This wake deficit generates unsteady forces when it is incident on the rotor blade, generating noise. The question addressed in this paper is whether these unsteady forces and hence the noise can be mitigated using appropriate introduction of unsteady boundary conditions, i.e., active control.

Active control refers to the process of external modulation of relevant parameters of a process in order to improve its performance. The proposed actuation method is articulation of the trailing edge of the stator, i.e., the stator tail, similar to an aileron on a plane, with the goal of reducing

[1] Corresponding Author, email: dopila@mit.edu

the unsteady forces and hence the noise. Many actuation technologies could provide this articulation, including those based on electromagnetics, piezoelectrics, and fluidics. The specific method investigated in this paper uses polypyrrole, a conducting polymer. The attractive features of such a method are its potential in realizing high power to mass ratio, high stresses, and low self noise production.

The specific conducting polymer material used in this work is polypyrrole, which like other conducting polymers, undergoes volumetric changes that allow it to perform as an artificial muscle [9]. This motion is caused by ion exchange with a surrounding electrolyte and yields stresses as high as 5 MPa with strains of 1-3% [9-13].

For tail articulation, the CP-based actuator is fabricated from polypyrrole using methods developed by MIT's Bioinstrumentation Lab [9,12,13]. The general actuator design is altered to suit the demands of this particular application. The actuator is fabricated 17 x 40 mm in size and constrained to curl only along its narrow dimension, the desired performance for this application. The polypyrrole actuator is encapsulated in plastic to allow immersion and operation in water. The operation of the actuator is tested and optimized for operation in water.

A benchtop open-channel water tunnel is used to study the flow around a stator with an articulated tail. The wake deficit is measured and compared for different types of tail articulation. Noise production is predicted by simulating a rotor blade passing through the stator wake.

In what follows, section 2 discusses the experimental setup. Section 3 discusses the two actuation methods, conducting polymers and the stepper motor, and their fabrication. The bandwidth and authority of these actuators in discussed in section 4. The experimental results of the flow testing are presented in section 5. Section 6 deals with the theoretical noise production and how it can be controlled.

2. EXPERIMENTAL TESTBED

Experiments were conducted in a small open channel water tunnel to study how the flow field can be changed by trailing edge articulation. An open channel water tunnel is used because of its simplicity; the purpose of this work is to generate proof of concept. The water tunnel (Armfield, Inc.) used in this work has a test section 40 cm long in the streamwise direction, 25 cm wide, and 4 cm deep. This tank is capable of speeds from 1-7 cm/s. These experiments were all conducted when operating at a constant 4 cm/s. A stator based on the NACA 0012 profile is used. The stator is 9 cm long with an articulated tail section 1 cm long, for a total chord length of 10 cm. This yields a Reynolds number of 4000. Velocity measurements were taken 0.8 chord length (8 cm) downstream from the stator assembly, as shown in figure 1.

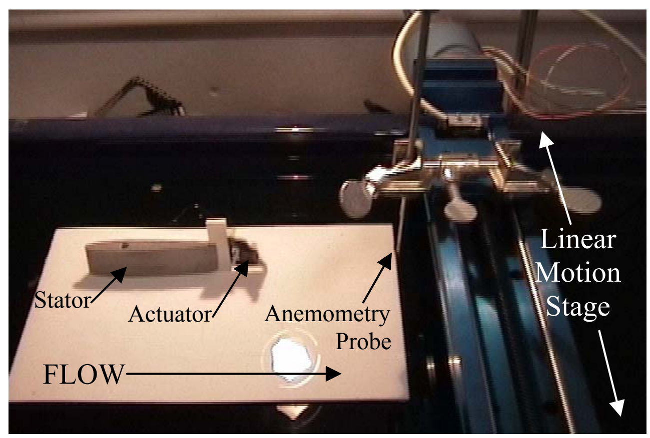

Figure 1: Experimental Testbed

To conduct measurements on the flow field, a hot film anemometry probe is mounted on a linear motion stage that spans the width of the tank downstream of the stator, allowing the probe to be moved across the tank.

Tail articulation is provided either by a conducting polymer actuator or a stepper motor attached to an aluminum tail section. The conducting polymer actuator (see section 3.1) is clamped in a groove machined in the back of the stator acts as the articulated tail, as shown in the figure. Two wires attached above the water line provide electrical power for the actuator.

The stepper motor and aluminum tail are used in place of the polymer bilayers for repeatability and to explore operation beyond the capability of the polymer (see sections 3.2, 5.3). The stepper motor is mounted out of the water directly above the tail pivot point, as shown in figure 2.

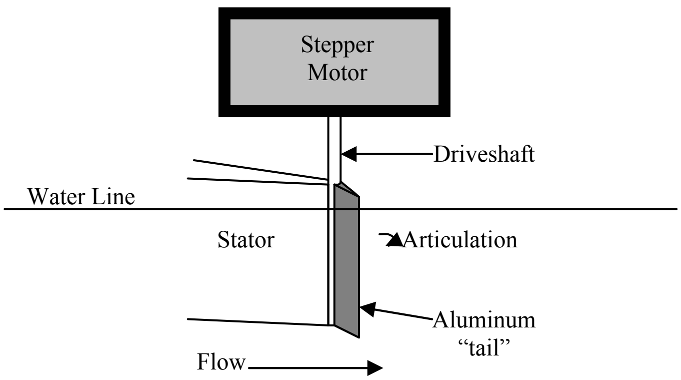

Figure 2: Tail articulation via stepper motor.

The stepper motor directly drives a shaft attached to the aluminum tail to provide articulation.

3. ACTUATOR DESIGN

This section discusses the design and fabrication of conducting polymer actuators (sec. 3.1.1), their encapsulation for operation in water (sec. 3.1.2), and the design of the stepper motor apparatus (section 3.2).

3.1 Encapsulated Conducting Polymers

3.1.1 Fabrication

The active material in the biomimetic actuator is polypyrrole, a conducting polymer. These organic polymer molecules contract when a potential is applied and ions from a surrounding electrolyte diffuse into the polymer. The polypyrrole is fabricated in thin films. When activated, these films contract uniformly in all in-plane directions, producing strains of ~2% [10-17] at strain rates of up to .1% s^{-1} [10,11] under normal conditions.

To provide a mechanical amplification of the small strains and strain rates to yield useable motion for this application, a bilayer is used. Two polymer films 20 microns thick are laminated together with a spacer in between to form a bilayer [17-21]. The small motion of the films relative to each other causes a bending of the bilayer, and a large amplification of the motion of the polymer films. However, this motion amplification causes a proportional loss of force. The bilayers studied in this paper are approximately 17x40 mm and 80 microns thick. This yields a bilayer that can bend as much as 180 degrees, but with a .1 N tip force. For this application, the bilayers are constrained to curl in only one direction.

Fabrication of a useable bilayer actuator involves three steps. Polypyrrole films must be synthesized to provide the raw material for the bilayer. The polymer films are then assembled in layers to form a bilayer capable of actuation. The actuator is then mechanically constrained to curl in a manner appropriate for this application. These three steps are described below. The final step is encapsulation in plastic to allow operation in water, which is described in section 3.1.2.

Polypyrrole Synthesis:

Hexafluorophosphate-doped polypyrrole films are grown from a solution of .06 M purified pyrrole monomer and .05 M tetraethylammonium hexafluorophosphate in propylene carbonate, using the methods of Yamaura [22] as previously described by others [17,23] as briefly described below.

The polypyrrole is deposited galvanostatically onto a polished glassy carbon beaker 75 mm in diameter and 82 mm high at a current density of 1.25 A m^{-2}. Deposition runs approximately 12 hours to yield films 20-25 micrometers thick. After deposition, the polypyrrole films are removed from the crucible by scraping them off with a razor blade. This yields films that look like black VHS recording tape, but are more fragile. The films are then coated in a solution of .05 M tetraethylammonium hexafluorophosphate in propylene carbonate and stored in plastic wrap or baggies.

The underlying cause for the motion of the polypyrrole is ion exchange with an electrolyte, so the polypyrrole films must be in contact with an electrolyte to operate. For this application an electrolyte based on an ionic liquid was used as described by Noda and Wantabe [23] as shown in table 1. This electrolyte is a liquid that forms a gel when baked at 85 C for 12 hours. The gel is applied to the desired surfaces, clamped, and then baked.

Table 1: BMIBF4 Gel Electrolyte Synthesis

Ingredients:	Mol %	Mass (g)
1-Butyl-3-methylimidazolium tetrafluoroborate (226.03 g/mol)	40	10.0
2-Hydroxyethyl methacrylate (130.14 g.mol)	58.4	8.41
Ethylene glycol dimethacrylate (198.22 g/mol)	0.8	0.175
Azobisisobutyronitrile (164.21 g/mol)	0.8	0.145

Gel Recipe courtesy of MIT's Bioinstrumentation Lab

Bilayer Fabrication:

To form the actuators, two polypyrrole films are separated by a sheet of lens paper [17] soaked in the BMIBF4 gel electrolyte to form the cross section shown in figure 3.

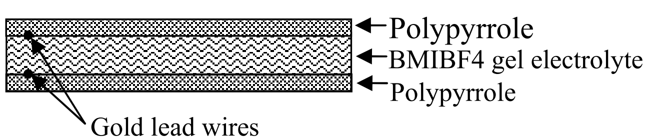

Figure 3: Cross section of bilayer actuator.

The lens paper serves as electrical insulation between the two sheets of conductive polypyrrole. The lens paper also acts as a lattice to absorb and hold the liquid electrolyte before it is baked to form a gel. Once this occurs, the gel serves as an adhesive and holds the bilayer together. Two gold wires run along one side of the bilayer between the lens paper and each sheet of polypyrrole as shown in the figure [24]. These wires serve as electrodes to provide electrical current to the polypyrrole films and to allow external electrical connections to be easily made with the bilayer. The bilayer is assembled in this configuration and clamped between two sheets of glass or Teflon. The assembly is then baked at 85 C for 12 hours.

This process yields a completed bilayer capable of motion. The bilayer is then trimmed using a razor blade to remove any excess material and bring the actuator to the desired size. The appropriate scale size for the actuator given the size of the stator model (10 cm long) is 16 X 40 mm.

Directional Actuation:

The polypyrrole films contract uniformly along in-plane directions, so the bilayers curl along all in-plane directions. This motion is undesirable for this application, since for the problem at hand, the bilayer should curl only along its narrow dimension in a fashion similar to a fish tail, as shown in figure 4.

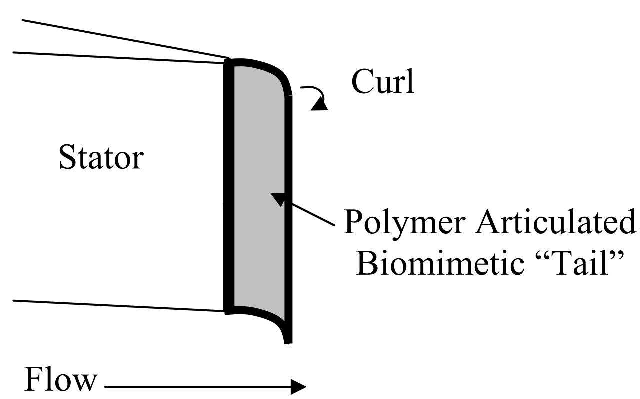

Figure 4: Desired behavior of the polymer tail.

To constrain the bilayer to curl in only one direction, mechanical stiffening strips are used. Several materials were tried, the most efficient of which are carbon fiber and muscovite mica [24]. Strips of material are glued along the long edges of the bilayer using a flexible urethane as shown in figure 5.

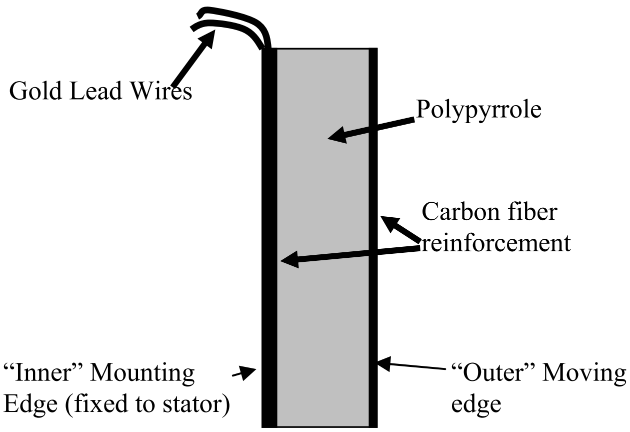

Figure 5: Stiffening strips constrain curl to only one direction

These strips constrain the bilayer and prevent it from curling along its long axis, leaving only the desirable curl across the narrow dimension. Overall, this method works well, but it does add some nonuniform thickness to the bilayer. The long edge of the bilayer can get out of phase and become twisted, but it stays straight and does not form undulations along its length.

Another method used to constrain the curl involved cutting slits along the narrow dimension of the bilayer. This relieves the stress along the long dimension of the bilayer and causes it to curl only across its narrow dimension. Small strips of bilayer are left intact at the edges to hold the bilayer together. This method worked nearly as well as the stiffening strips, but minor electrical shorts and other problems caused difficulties. We refer the reader to [25] for further details.

3.1.2 Encapsulation

The final step in the CP actuator design for this application is encapsulation in plastic to allow operation in water. The polymer films must be protected from water intrusion, loss of electrolyte, mixing with other solvents, and contamination from ions in the environment. Two methods of encapsulation are primarily used that form a protective plastic envelope around the bilayer [9]. Two types of clear plastic film are used for either method: polyethylene terephthalate (PET) and polyvinylidene chloride (PVDC, available as Saran Wrap™). The PVDC is 13 microns thick while the PET used is 6 or 13 microns thick.

The first method uses a flexible urethane adhesive with a folded plastic film [24]. The bilayer is laid flat on the plastic film and surrounded on three sides by a thin band of urethane on the plastic. The two part urethane is mixed and applied using a wire similar in size to a toothpick. The urethane is scraped to yield a very thin, consistent layer. The outside long edge of the bilayer receives no adhesive. The plastic is then folded over the outside edge of the bilayer and onto the urethane to form the envelope. This leaves an envelope with one edge as a fold and the other three sides sealed with urethane. In one variant of the procedure, a syringe needle is placed inside the envelope as it is formed. The needle is used to draw a vacuum inside the envelope and then removed. This vacuum eliminates air bubbles inside the envelope and pulls the plastic flush against the actuator. After the urethane has cured, excess urethane and plastic is cut away with a razor blade to leave a 3mm band of urethane and plastic that seals the edges of the envelope.

The second method uses a spray adhesive in place of the urethane. A sheet of plastic film is laid on a sheet of glass to hold it flat and smooth. 3M 77 general purpose adhesive is applied to the plastic in 5-10 thin coats using a mask to prevent undesirable adhesive application. As it is a tack adhesive, the adhesive is allowed 1 minute to dry between coats. After the adhesive application, the bilayer is situated such that there is a band of adhesive around all four sides. A second sheet of plastic is held smooth with no wrinkles and placed down on top of the bilayer and the first sheet of plastic. Any air bubbles or wrinkles are pressed out. The excess plastic is trimmed away to leave a 4 mm band of adhesive and plastic around the edges of the bilayer.

Both encapsulation methods produce an actuator that will function in shallow water. The water tunnel in this work is 2.5" deep, so functionality at 3" deep or less is the goal. The urethane adhesive has higher peel strength than the spray adhesive, yielding a more durable actuator, but its application methods and stiffness cause problems. When applying the urethane adhesive it is difficult to form a very smooth, even, consistent layer. This translates into inconsistencies in the adhesive band in the finished actuator. The urethane band is applied thicker than it should be to account for inconsistencies and prevent leakage in the finished product. This is a major problem because the stiffness of the urethane band changes with the cube of the thickness. The inconsistencies in the urethane process yield an encapsulation envelope that is mechanically stiffer than it needs to be.

The spray adhesive method is used to solve two main deficiencies in the urethane adhesive method: the thickness of the adhesive and inconsistencies in its application. A spray-on adhesive is ideal to solve these two problems; it is applied in very thin, uniform coats. The thickness is controlled to provide sufficient water protection without using excess adhesive. The disadvantage of the spray adhesive is that it has lower peel strength than the urethane. While this was not a factor for the actuators in this work, actuators in deeper water may require the better protection of urethane or another adhesive.

3.2 Stepper Motor

Due to the difficulties involved in using polymer actuators, including bandwidth limitations, another actuation method based on a stepper motor was also used in order to study the flow characteristics. A stepper motor was used because of its simplicity and large available bandwidth. The motor used was an "Mdrive 17" manufactured by Intelligent Motion Systems, Inc. It is mounted above the waterline directly over the pivot point of the tail. A drive shaft attached to an aluminum "tail" section is directly attached to the motor output shaft (see figure 2). This drive shaft sits at the trailing edge of the stator model and serves as the hinge and transition between the stator section and the articulated tail section. By design, this drive shaft is as wide as the stator thickness where it is mounted, 90% of the chord length from the leading edge of the stator. This leaves the articulated surface as 10% of the chord length of the stator.

4. ACTUATOR PERFORMANCE: BAND-WIDTH AND AUTHORITY

Since the intended use of the tail actuators is temporal articulation with sufficient bandwidth for noise reduction, we need to ascertain the available authority of the actuator and thus its available motion. This section discusses the actuation available from the polymer actuators (sec. 4.1) and the stepper motor (sec. 4.2).

4.1 Bilayer CP

In this section we document the performance of the CP bilayer actuators. A CP actuator of size 17 x 44 mm fabricated using the methods of section 3.1 is mounted on the trailing edge of a stator and the assembly placed in water. The actuator is driven with a 2 volt square wave (4 volts p-p), and the maximum tip deflection is measured from the neutral position. The frequency of this source voltage is shown on the horizontal axis in figure 6 below.

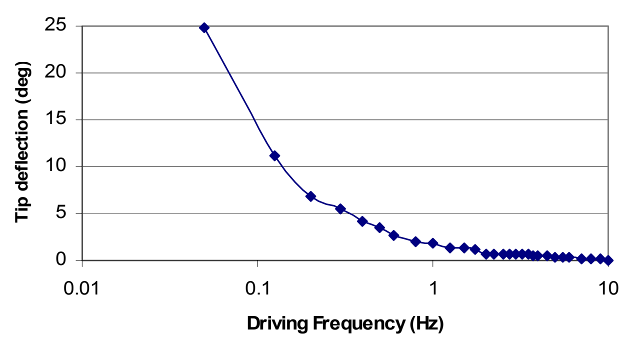

Figure 6: Typical encapsulated actuator performance.

Figure 6 shows that the actuation performance of the encapsulated conducting polymer actuators is the limiting factor in their use. The actuators can achieve large (~25 degree) tip deflections from neutral, but only at slow speeds. The actuators can move relatively quickly around the neutral position, but slow down as they achieve larger deflections. Their original low bandwidth of approximately 1 Hz and authority of 4 degrees tip deflection are further compromised by the plastic encapsulation.

Due to the small tip forces available (.1 N) the deflection of the actuators is measured using a video camera. The actuator is filmed in front of a ruler while oscillating and the film is analyzed to provide an estimate of tip deflection. The curvature of the bilayer is the ideal parameter to be measured; the bilayer actually induces tip motion by causing a curvature. However, the curvature is not uniform along the length of the bilayer, making it difficult to measure. Tip deflection is much easier to quantify and still gives a useful estimate of the performance of the actuator, especially at small deflections.

4.2 Stepper authority

The stepper motor and controller used in these experiments was sufficiently powerful to provide speeds (>300 rpm) well beyond the needs of this application.

5. ACTUATOR IMPACT ON FLOW FIELD

As the primary goal of tail articulation is noise reduction, the tail motion must somehow alter the flow field in order to alter or reduce the radiated noise. Thus, the tail articulation is quantitatively evaluated for its potential to alter the flow field by measuring the velocity field in the open channel water tunnel.

This section describes the undisturbed flow (sec. 5.1), and changes in the flow field that result from both the polymer actuators (sec. 5.2) and the stepper motor (sec. 5.3). Section 5.3 is further divided into the actual velocity measurements (sec. 5.3.1), the Strouhal numbers for effective operation (sec. 5.3.2), and a comparison of the polymer and stepper motor performance (sec. 5.3.3).

All measurements in this section are taken 80% (8cm) of stator chord length downstream from the trailing edge of the stator/actuator at a free stream velocity of 4 cm/s. All length dimensions are normalized against the stator chord length. The spanwise position across the tank is expressed as

$$y' = \frac{y}{L} \qquad (1)$$

where y is the spanwise position perpendicular to streamlines in the tank, and L is the stator chord length. The motion of the tail articulation is normalized as

$$D' = \frac{t_d}{L} \qquad (2)$$

where t_d denotes tail deflection. The streamwise velocity U is normalized against the free stream velocity U_o

$$U' = \frac{U}{U_o} \qquad (3)$$

5.1 Baseline measurements

As previously mentioned, a hot film anemometry probe is used to measure the flow field as the tail is articulated. To obtain measurements at more than one position to yield velocity data in both time and space, the probe is moved to a number of different positions. At each position, the tail is moved according to a specified motion profile and the velocity measurements are recorded. The data from multiple points are combined so they are all in phase with regard to the position of the tail. This yields data across the width of the tank as the tail moves along its profile. In using this method, one assumes that the same velocity field is repeated each time the tail motion is repeated. The experiments conducted were found to be repeatable, so this assumption is valid.

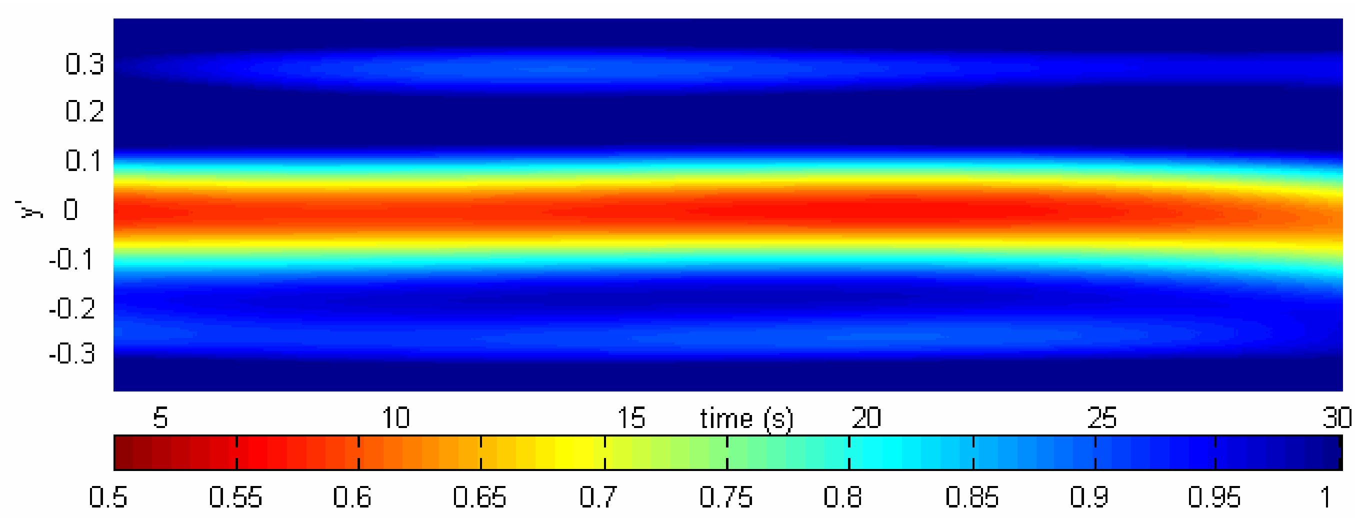

Figure 7: Baseline streamwise velocity *U'* at 80% of chord length downstream of a stator with no trailing edge articulation, shown as a function of *y'* and time.

In order to have a baseline for comparison, the flow field was measured with the stator and actuator in the water, but with no articulation, as shown in figure 7.

The band of slower velocity (*U'*=0.55, compared to U_o'=1) at zero position illustrates the wake deficit from the stator. The free stream velocity appears on the edges of the figure to either side of the central wake deficit. As expected, the wake deficit is approximately constant in width and magnitude. The minor nonuniformities and fluctuations are due to measurement error and appear in all the experiments.

5.2 Impact of CP-based articulation

An encapsulated CP actuator is mounted at the trailing edge of the stator in water. The velocity is measured at a single position directly behind the actuator and 80% of chord length downstream. This experiment was conducted only to show that the CP actuators can alter the flow to some extent, so 2-D measurements were not carried out.

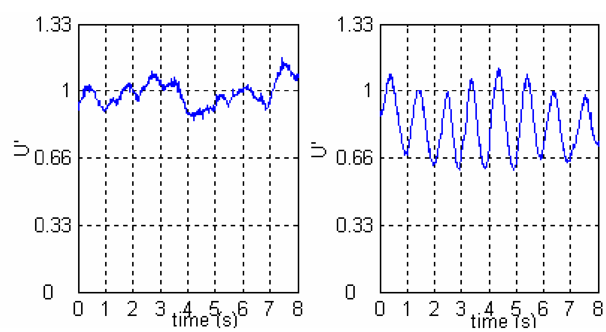

(a) (b)

Figure 8: Flow alteration due to bilayer oscillation (a) without articulation and (b) with polymer articulation at 1 Hz.

Figure 8(a) shows the baseline water velocity of 4 cm/s with the actuator in the water but without actuation. The oscillations in the left plot are due to measurement error and small variations in tank speed. The plot on the right shows the velocity during actuator motion, a velocity fluctuation at the same frequency as the actuator motion. The velocity profile matches the actuator excitation frequency in the range of .1-2 Hz for tank speeds from 1 to 6 cm/s. From these observations, it can be assumed that the velocity fluctuations are caused by the bilayer motion. These experiments show that the bilayer actuators can modify the water flow at these speeds despite their low tip force.

5.3 Impact of stepper motor articulation

5.3.1 Flow Characteristics

Since the stepper motor has significantly more authority than the polymer based actuators, large classes of tail articulation can be imposed on the tail. In what follows, we present the results from four specific articulation profiles that capture the overall impact of stepper motor based tail articulation. In all cases, as in section 5.2, the velocity is measured at a single position directly behind the actuator and at 80% of the stator-chord length downstream.

The first tail motion profile is a simple sinusoid of period 2π s (0.159 Hz) and amplitude 1 rad., as shown in figure 9. The position of the actuated tail is shown in figure 9(a) with the corresponding velocity shown beneath in 9(b). For this tail motion, the wake deficit appears to move with the tail. The wake deficit remains approximately constant in width and magnitude, but shifts back and forth across the tank with the tail.

This agrees with the expectation that the momentum deficit generated by the stator cannot be easily compensated for. The tail motion begins at 10 seconds, but its effects are not visible until 4 seconds later due to the convective delay. In general, this tail motion is rather slow but has a large deflection (57 degrees) and appears to easily shift the wake deficit.

Profile #	Type	Amplitude (rad)	Frequency (Hz)
1	Sinusoid	1	0.159
2	Sinusoid	0.5	0.318
3	Sinusoid	1	0.636
4	Transient	~.8	~.2

Table 2: Tail articulation profiles used for wake deficit alteration.

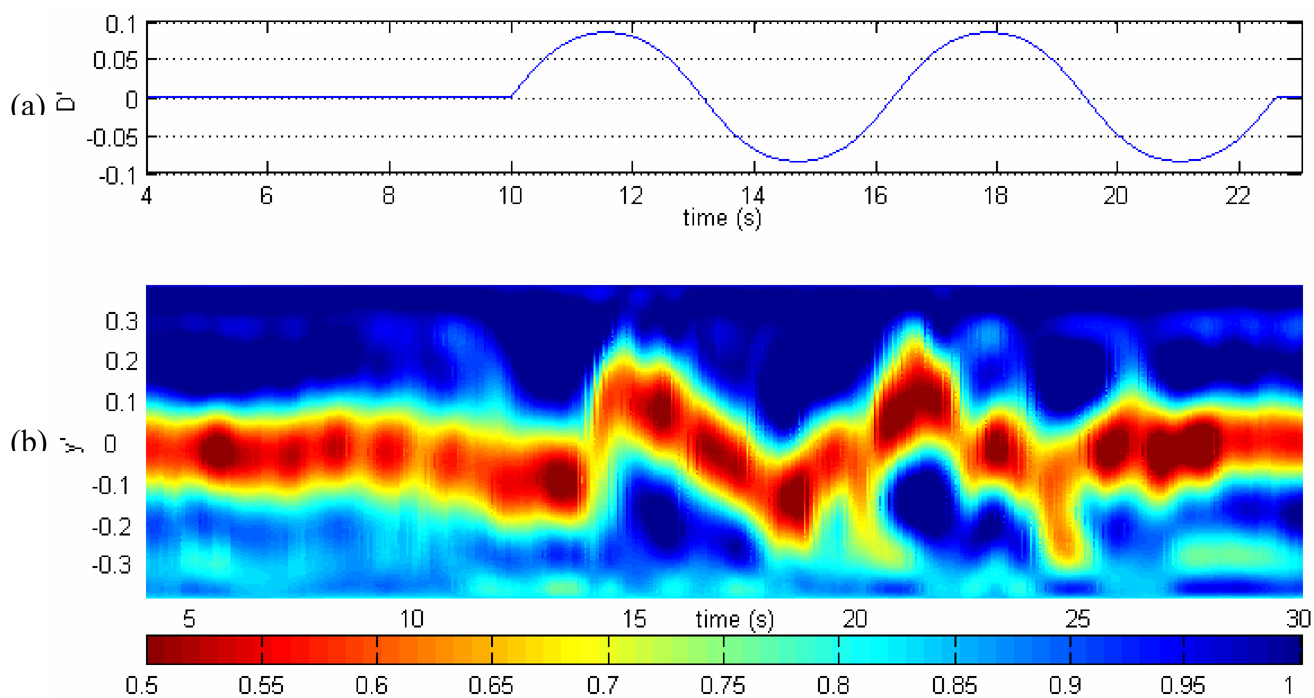

Figure 9: Flow field with move profile 1 showing (a) tail tip displacement *D*' and (b) *U*' as a function of *y*' and time

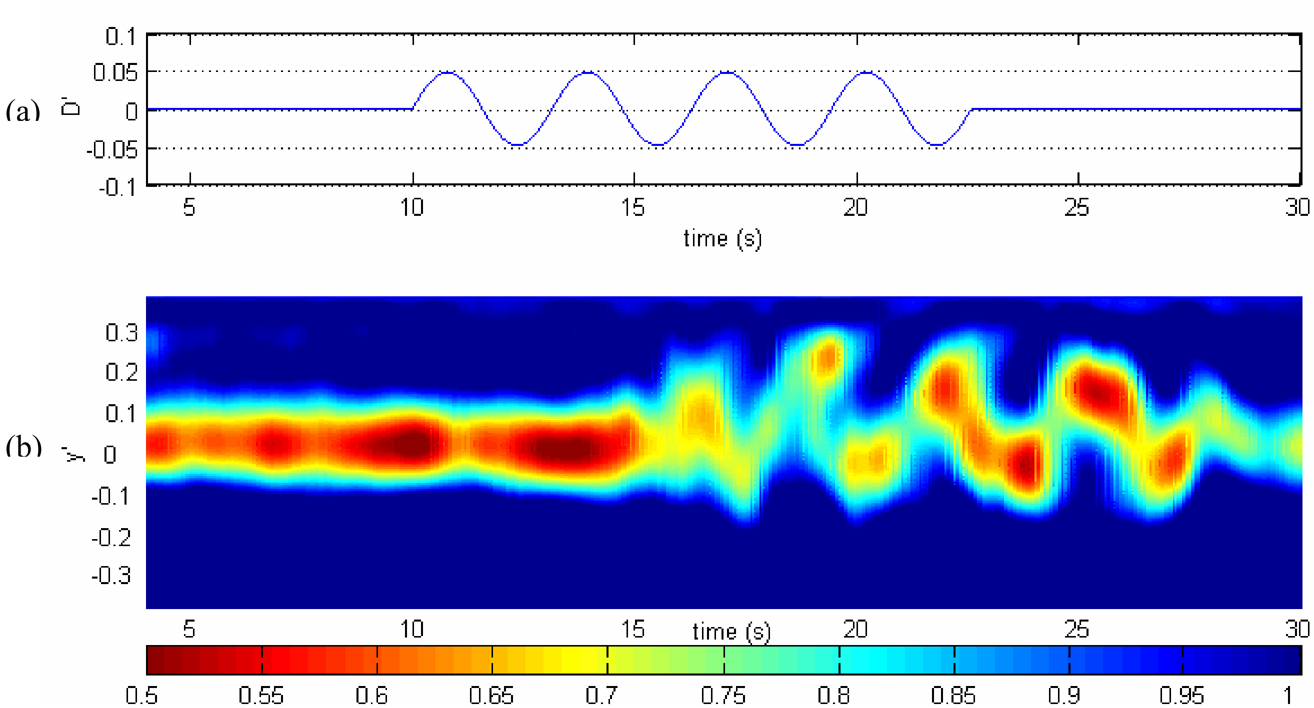

Figure 10: Flow field with move profile 2 showing (a) tail tip displacement *D*' and (b) *U*' as a function of *y*' and time

The next tail motion used is again a simple sinusoid, but with twice the frequency (0.318 Hz, period π) and half the amplitude (0.5 rad. deflection), as shown in figure 10(a). This faster oscillation changes the velocity field significantly. The wake deficit can still be seen to oscillate back and forth, but its magnitude decreases by approximately 40%, from time 17 to 21 seconds. The deficit approaches its typical magnitude again around 23 seconds, although it is still significantly disturbed. The temporary wake deficit reduction is likely due to startup transients involved with the tail motion. These observations are difficult to reconcile with conservation of momentum arguments. It would appear the deficit is spreading over a wider portion of the tank and thus the velocity can be lower while still conserving momentum, or other phenomena are involved.

It is interesting to note that the deficit seems to be lowest when the tail is at its neutral position (after accounting for the convective delay) and moving at its fastest. When the tail pauses at either end of its oscillation, the deficit grows to approach its baseline value. This can be seen as the two lower velocities (*U*'=0.6) visible at 20 seconds. These lower velocities occur at the edges of the tail travel. From this observation, it seems that the deficit reduction is realized due to the actual motion of the tail segment and not during a mere displacement from neutral. It appears that tail tip speed is the most important parameter concerning wake deficit alteration.

The next experiment was conducted to test faster large amplitude tail oscillations. A simple sinusoid is again used with period π/2 (0.636 Hz) and amplitude 1 rad. as shown in figure 11. This tail motion has an undesirable effect. The wake deficit actually increases and becomes convoluted. The oscillations appear to be too fast for this tank speed, and hence any effect the tail has is "smeared" again by the tail before it has a chance to convect downstream. This implies that there is an upper limit to the frequency of effective desirable wake alteration. Given the observation that deficit reduction occurs during tail motion, a new profile was designed. Previous work [8] shows the theoretical potential for noise reduction by imparting a point circulation at the trailing edge of the stator. The required command input has three identifiable characteristics: one relatively large initial displacement that settles out, a zero crossing, and a settling time less than the blade passing frequency. Using these characteristics, the move profile for the position of the "tail" was designed as shown in figure 12(a).

The amplitude and frequency of this tail motion (fig 12(a)) were chosen so that they result in the optimal drop in wake deficit. This move profile has speeds similar to move profile 1 (Fig. 9) with slightly smaller amplitude and higher frequency. The tail motion settles out after approximately 8 seconds. This causes the wake deficit to shift up, down, then neutral (fig. 12(b)) as expected. However, as the tail shifts back across the neutral position from top to bottom, there is a slight drop in the wake deficit from time 16 to 18 as shown by the faster flow (*U'*=0.65) during that time. In addition, there appears to be a "gap" in the wake as it becomes partially discontinuous at 15-16 seconds as seen by the sudden increase in flow speed (*U'*=0.82). This drop could be exploited especially well if the blade were to be timed properly and pass through this gap. The implications of such a control are discussed in section 6.2.

5.3.2 Optimal Strouhal Numbers

The flow testing results show that wake deficit is reduced for a wide variety of frequency, amplitude, starting position and type of tail motion. There are no immediately identifiable trends that indicate which parameters influence this phenomenon. To better understand the mechanisms behind this reduction, a dimensionless quantification of the flow characteristics using the Strouhal number is provided in this section.

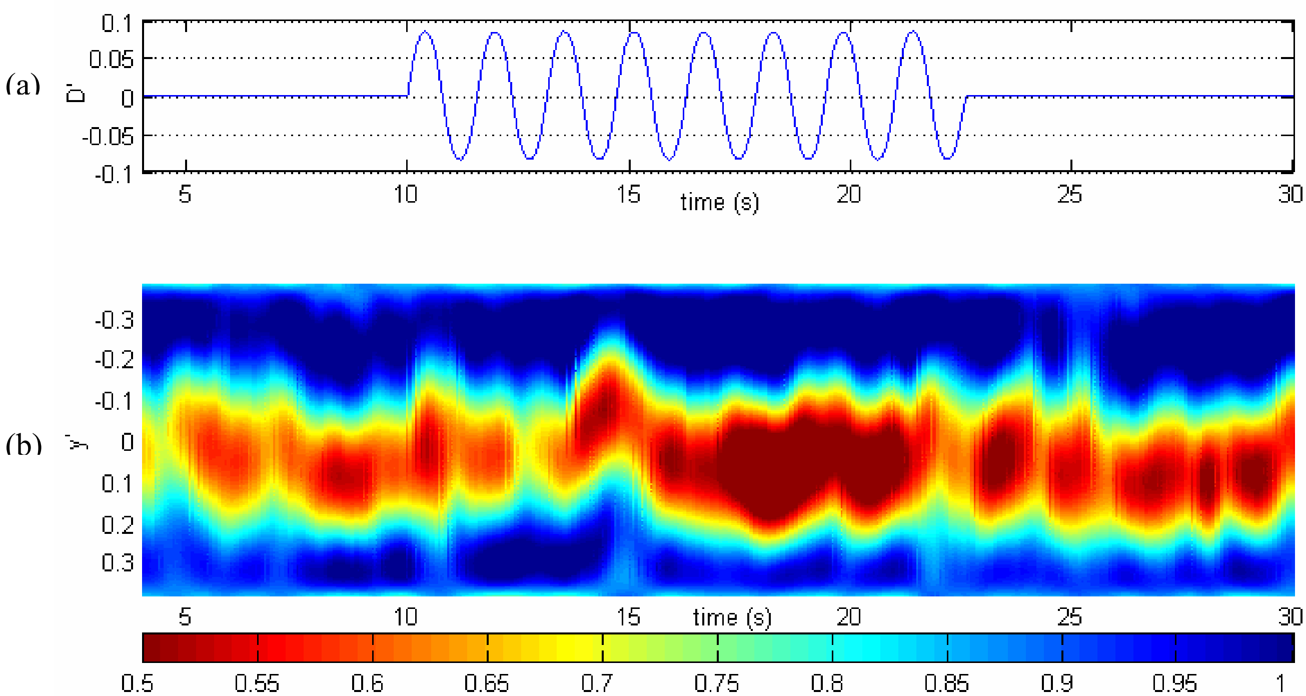

Figure 11: Flow field with move profile 3 showing (a) tail tip displacement *D*' and (b) *U*' as a function of *y*' and time

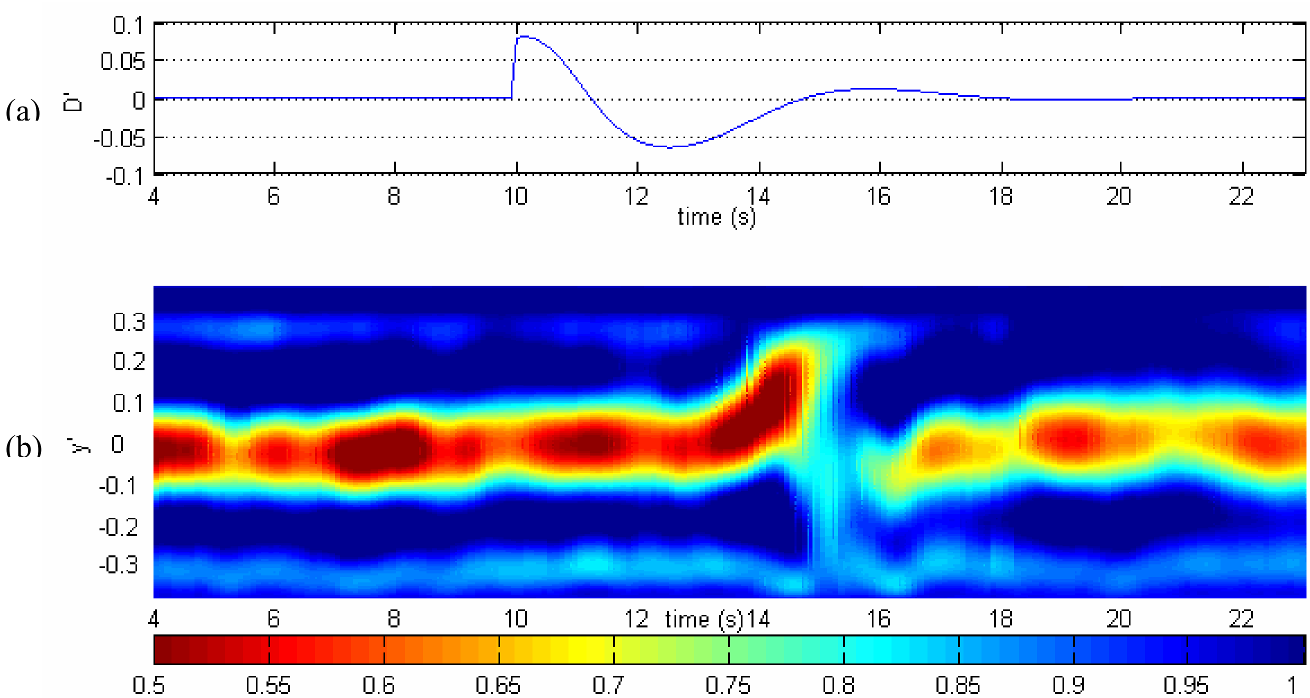

Figure 12: Flow field with move profile 4 showing (a) tail tip displacement *D*' and (b) *U*' as a function of *y*' and time

The Strouhal number is defined as

$$St = \frac{fD}{U} \qquad (4)$$

where f is frequency of tail motion, D is wake width, and U is flow speed. The width of the wake is measured from a plot similar to figures 9(b)-12(b).

The normalized wake deficit reduction is defined as

$$\Delta W = \frac{Min_t\left(W_{d,uncon}\right) - Min_t\left(W_{d,con}\right)}{Avg_t\left(W_{d,uncon}\right)} \qquad (5)$$

where $W_{d,uncon}$ and $W_{d,con}$ denote W_d in the uncontrolled and controlled cases, respectively, and W_d is the maximum wake deficit measured spanwise at a point 80% stator chord-length downstream. We note that the wake deficit w_d at any point is given by

$$w_d(t) = U_0 - U(t).$$

The results of these comparisons are shown in figure 13.

The wake deficit is reduced most effectively for Strouhal numbers between 0.25 and 0.35, shown as dotted lines in figure 13(a). This is the theoretical optimal range previously predicted and observed by others for propulsion efficiency in fish and "RoboTuna", a motorized Bluefin [7]. Their research shows that fish use a complex interaction of vortices to generate efficient thrust (fig 13(b)). Our results show that the operating regime for optimal wake deficit reduction is similar to that for propulsion efficiency, with an almost identical optimal range of Strouhal numbers.

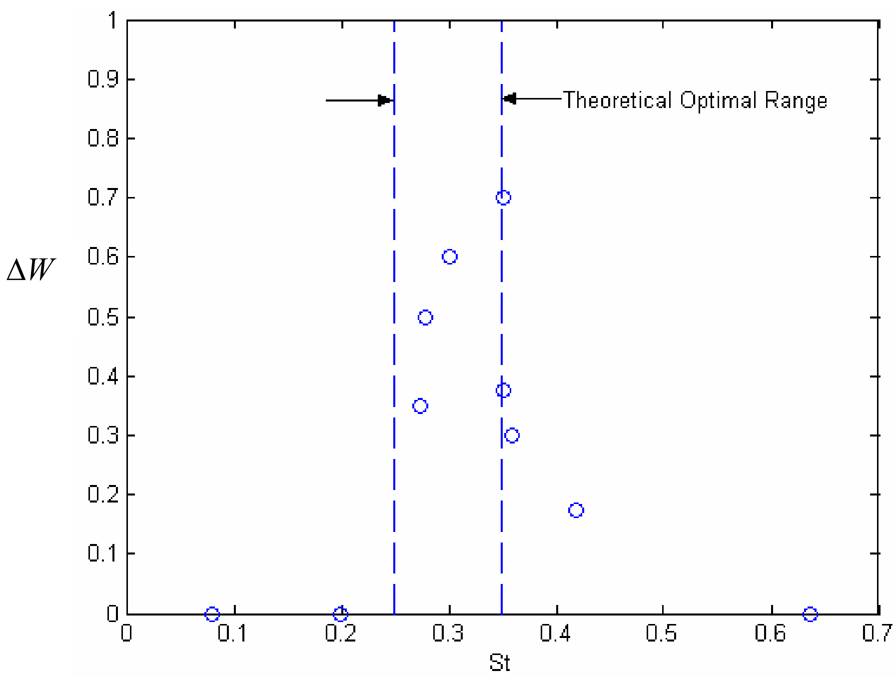

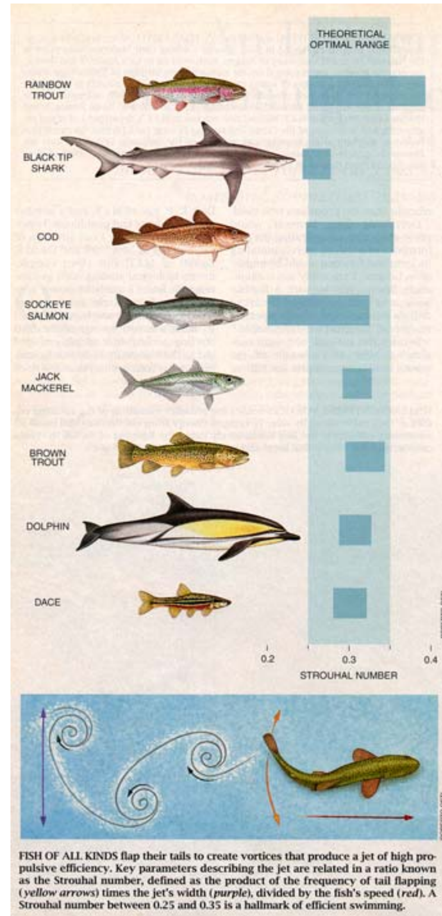

(a) Wake Deficit Reduction *ΔW* as a function of the Strouhal Number

(b) Propulsion Efficiency as a function of Strouhal Number [7]. *Reprinted with permission from Scientific American*

Figure 13: Wake deficit reduction as a function of Strouhal number.

5.4 Conducting Polymer vs. Stepper Motor Performance

The flow testing using stepper motor actuation shows the potential for wake deficit reduction. Conducting polymer actuators are being investigated for use in this application, so their performance is compared to that required for wake deficit reduction.

Figure 14 shows the minimum tail motion required to produce a wake deficit reduction and the available polymer deflection at that frequency. The required tail motion is shown as a solid line while the available polymer deflection is represented by the dashed lines. The polymer actuators can achieve approximately 40% of the required motion for wake deficit reduction at this tank speed (4 cm/s), and hence are still not adequate for this application.

6. PROJECTED IMPACT ON STEALTH

This section describes the possible noise reduction due to trailing edge articulation. Noise and force measurements were not made; a rotor

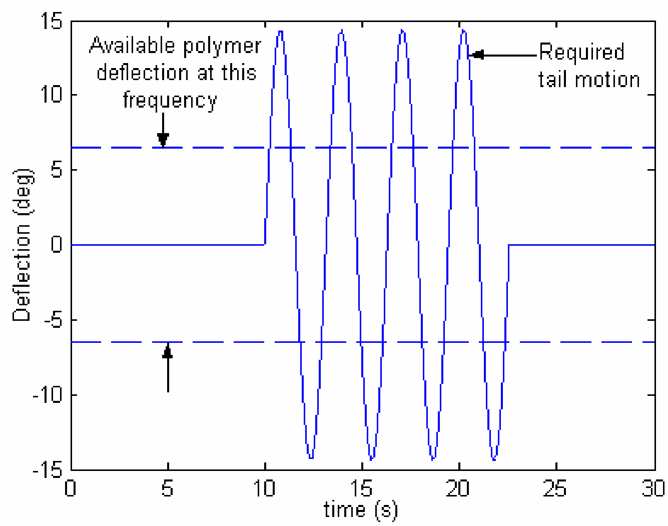

Figure 14: Minimum required motion for wake deficit reduction and available polymer deflection.

blade is simulated to pass through the experimentally measured velocity field. The noise model is briefly discussed in section 6.1 and the sound pressure levels are predicted in section 6.2. The power spectrums of the radiated noise are presented in section 6.3, and section 6.4 quantifies the sensitivity of the noise production to control input timing.

6.1 Motivation/noise model

The noise production was simulated using a previously developed noise production model [8], which makes the following assumptions:

- The effect of rotor-blade motion upstream on the vortices near the stator is negligible.
- All spanwise sections of the stator blades are assumed to move in phase (thereby allowing a two-dimensional analysis).
- No attempt was made to characterize the often more substantial indirect radiated noise, which is transmitted through structure and re-radiated elsewhere from the location of the unsteady force.

Fortunately, in practice, a reduction in direct radiation leads to a reduction in indirect radiation as well. Consequently, attempts to reduce unsteady forces are assumed to be more meaningful than addressing all noise source reductions explicitly [8].

The noise model is normalized along the chord of the rotor. ξ is the normalized chordwise coordinate along the rotor airfoil section, which varies between −1 and +1, with $\xi = 0$ corresponding to the rotor midchord. V_{tn} is the velocity normal to the blade pitchline and can be calculated based on the blade pitch angle β.

$$V_{tn} = U(x,y,t)\cos(\beta) + V(x,y,t)\sin(\beta) + \Omega\sin(\beta) \qquad (6)$$

where *U(x,y,t)* is the streamwise velocity measured in the experiments, Ω is the rotor rotational frequency times the radius of the point in question from the centerline, and *V(x,y,t)* is the velocity component normal to the streamlines.

The maximum perturbation in the *y* direction occurs at the tip of the tail when it is moving fastest, which is at 2 cm/s, which implies that *V*~2 cm/s; in comparison, the streamwise velocity *U* is 4 cm/s. Also, the blade pitch angle is small (β=11.5°). In addition, the velocity measurements and theoretical blade passes occur eight tail chord lengths downstream; perturbations perpendicular to the streamlines likely decrease as they flow downstream. Hence, $V\sin\beta$ is neglected because its maximum value is small (10%) compared to $U\cos\beta$.

Defining V'_{tn} to be the unsteady component of lift and the transverse gust, the lift per radial distance can be expressed as:

$$L = \int_{-1}^{+1} g_1(\xi)\left[0.5 + \frac{0.5z}{s+z}\right] V'_{tn}(t)d\xi + \int_{-1}^{+1} g_2(\xi)\dot{V}'_{tn}(t)d\xi, \qquad (7)$$

with

$$g_1(\xi) = 2\rho U_r l\left(\frac{1-\xi}{1+\xi}\right)^{0.5}$$

$$(8)$$

$$g_2(\xi) = 2\rho l^2(1-\xi^2)^{0.5}$$

$$U_r = \sqrt{U^2 + \Omega^2} \quad (9)$$

$$z = \frac{0.3\sqrt{0.5}U_r}{l} \quad (10)$$

where U is the free stream velocity, ρ is fluid density, and l is the rotor chord length. Once the lift force L is computed, the pressure component due to direct radiation can be calculated using Lighthill's equation. This yields the acoustic (unsteady) component of pressure p' at a given position relative to a varying force due to the direct radiation to be proportional to that varying force [26].

$$p'(\vec{r},t) = \frac{\dot{F}(t')}{4\pi r c_o}\cos\theta \quad (11)$$

where $F(t')$ is the total fluctuating force, r is the distance to the field point being calculated, c_0 is the speed of sound, $t'=t-r/c_0$, and θ is the angle between the force vector and the direction to the field point for which the pressure is being calculated. Equation (11) is simplified for this application as

$$p' = k_0\dot{L} \quad (12)$$

where $\dot{L}$ is the time derivative of the lift force, and k_0 is a suitably chosen constant.

6.2 Noise predictions

In this section, we present the results obtained using the noise model in section 6.1 and the velocity fields from move profiles 2 and 4 (figs 10 and 12). The results obtained are presented in figures 15 and 16 respectively. The data in both figures were obtained by keeping the tail stationary from 0 to 10 seconds, moving the tail using the profile of choice, and keeping the tail fixed from 23 to 30 seconds. In the case of move profile 4, it is assumed that the timing of the tail articulation is such that the rotor blade passes through the "gap" in the wake.

In order to calculate the radiated blade noise, it is assumed that a rotor blade moves through the flow field measured during tail articulation. The first noise experiment used the simplest actuation, a constant amplitude sinusoid (move profile 2) as shown in figure 10. The noise produced during the rotor blade travel can be seen in figure 15.

The paths of the virtual blades are shown in black on the velocity field (fig 15(a)). It follows that the first blade passes through the undisturbed wake, producing a baseline uncontrolled noise. The second blade passes through the wake during the initial startup transient (see section 5.3.1) of the tail motion, causing a 40% reduction in sound pressure level. The third blade passes through the wake after the startup transients have dissipated, but the wake is still disturbed and slightly reduced. In figure 15(b), the third blade pass appears to produce slightly more noise than the second, but its peak to peak amplitude is similar. In general, subsequent blade passes produce noise similar to that of the second blade pass.

Using a transient tail motion (profile 4), the sound pressure level for the controlled blade pass is approximately 60% less than the two uncontrolled cases, as can be seen in the figure 16(b). The velocity field is the same as shown in figure 12 and the blade paths are again shown in black. The control is active between 12 and 17.2 seconds (black lines in fig. 16(b)) after accounting for convective delay. The first and third blades pass through the undisturbed wake and generate uncontrolled noise. The second blade passes through the "gap" in the wake generated by the tail motion (see fig. 12). It is assumed that the timing of the tail articulation is such that the blade will encounter this "gap".

(a)

(b)

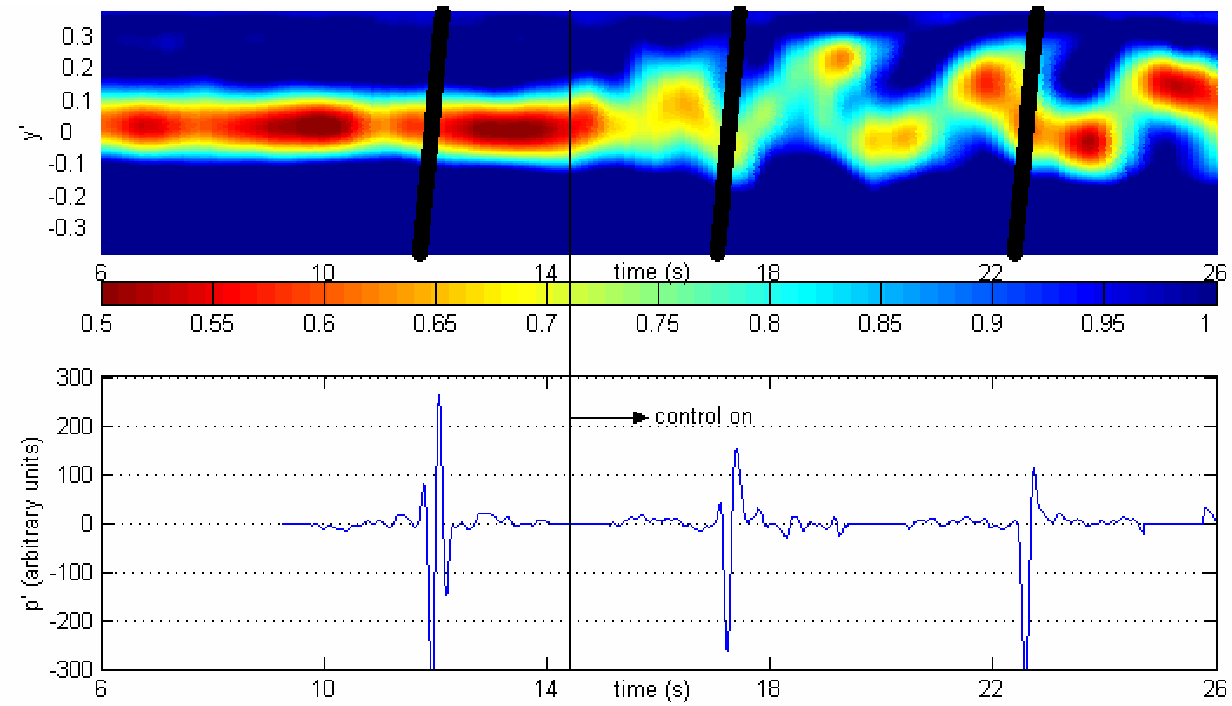

Figure 15: Radiated Noise for move profile 2: (a) Streamwise velocity *U'* with rotor blade paths shown in black (b) Predicted radiated noise.

(a)

(b)

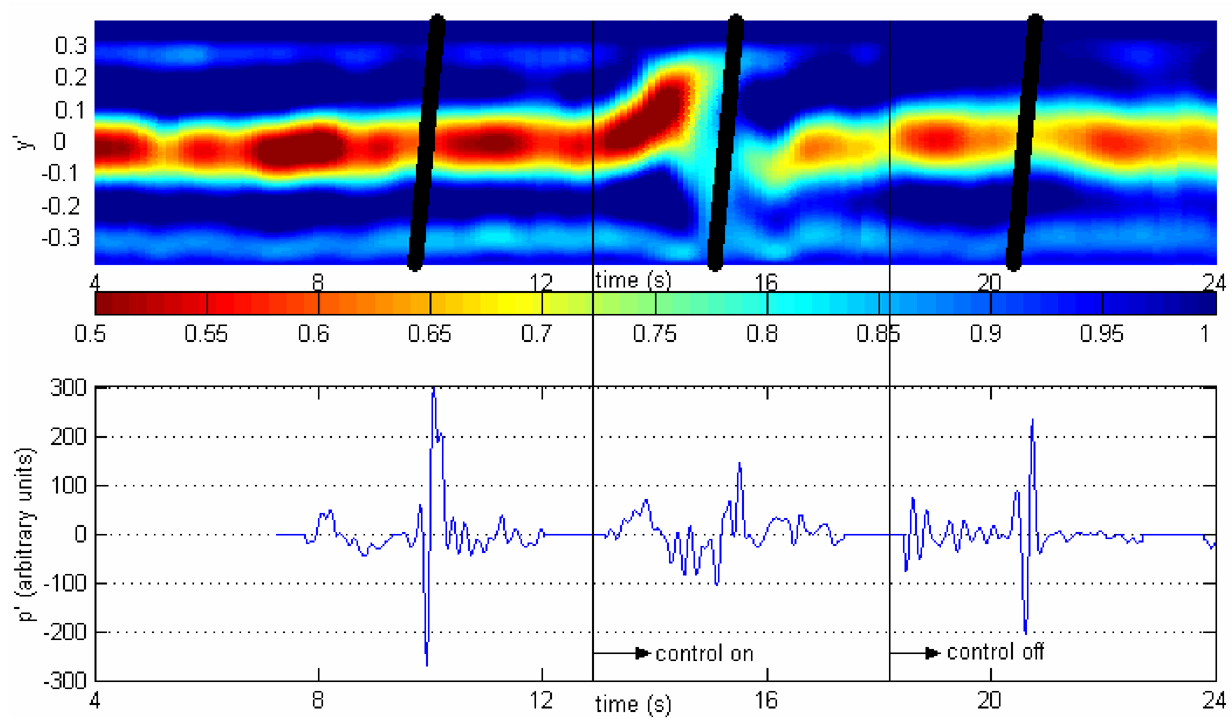

Figure 16: Radiated Noise for move profile 4: (a) Streamwise velocity *U'* with rotor blade paths shown in black (b) Predicted radiated noise

6.3 Performance Characterization in the Frequency Domain

We compare the performance of the tail motion profiles 2 and 4 in the frequency domain in figure 17.

The FFT for uncontrolled noise was standardized across different experiments to provide a uniform baseline and is shown in figure 17(a). Power is in units of dB SPL with an arbitrary reference pressure. (Power is magnitude squared, so a 6 dB SPL increase corresponds to a factor of 2 increase in sound pressure.)

The first controlled case uses the sinusoidal tail motion visible in figure 10, generating the noise shown in figure 15. The power spectrum of this noise is shown above in figure 17(b). This power spectrum is for the noise generated during the second blade pass shown in figure 15(a).

As previously mentioned, the sound pressure plots in figure 15(b) seem to indicate that the second blade pass has a more effective noise reduction than the third blade pass due to startup transients. This seems to be an aberration for that particular blade pass; for additional blade passes, the power spectrum is nearly identical to that shown above (fig. 17(b)) for blade pass 2.

To yield even greater reductions in noise production, a transient tail motion was used (fig 12,16). The noise spectrum for the second blade pass from figure 16(a) is shown in figure 17(c).

This transient tail motion reduces noise much more effectively (6-25 dB SPL in general) than the constant tail oscillations by taking advantage of unsteady flow characteristics. In calculating the noise spectrum for this transient tail motion, it is assumed that the control motion will be repeated and synchronized in the proper phase for each blade passing. This means the tail articulation must act, settle, and reset for each blade passage. While this is reasonable in these experiments, it may prove difficult in real applications. If this is the case, a constant tail oscillation still reduces noise as shown in figure 17(b). With the Overall Sound Pressure Level (*OASPL*), defined as

$$OASPL = \int Power(\omega)d\omega$$

and the OASPL reduction as ΔOASPL, where

$$\Delta OASPL = OASPL_{controlled} - OASPL_{uncontrolled}$$

with $OASPL_{uncontrolled}$ and $OASPL_{controlled}$ denoting the *OASPL* levels in the uncontrolled and the controlled cases, respectively, we obtained ΔOASPL=3db for the sinusoidal articulation, and ΔOASPL=6db for the transient articulation.

6.4 Sensitivity Studies

As discussed in section 6.2 in figure 16, noise reduction is dependent on time of blade pass. Denoting the optimal time of blade passing as t_0, we now study the robustness of the method assuming a single blade pass occurs at time $t_0 + \delta_0$, by calculating ΔOASPL with respect to perturbations δ_0 in t_0.

As the mechanism for noise reduction characterized in this paper is based in the flow field and not on any blade parameters, a disturbance in the start time of control is normalized in reference to the flow as

$$\delta_0' = \frac{\delta_0}{t_c} \quad (13)$$

where

$$t_c = \frac{L}{U_o} \quad (14)$$

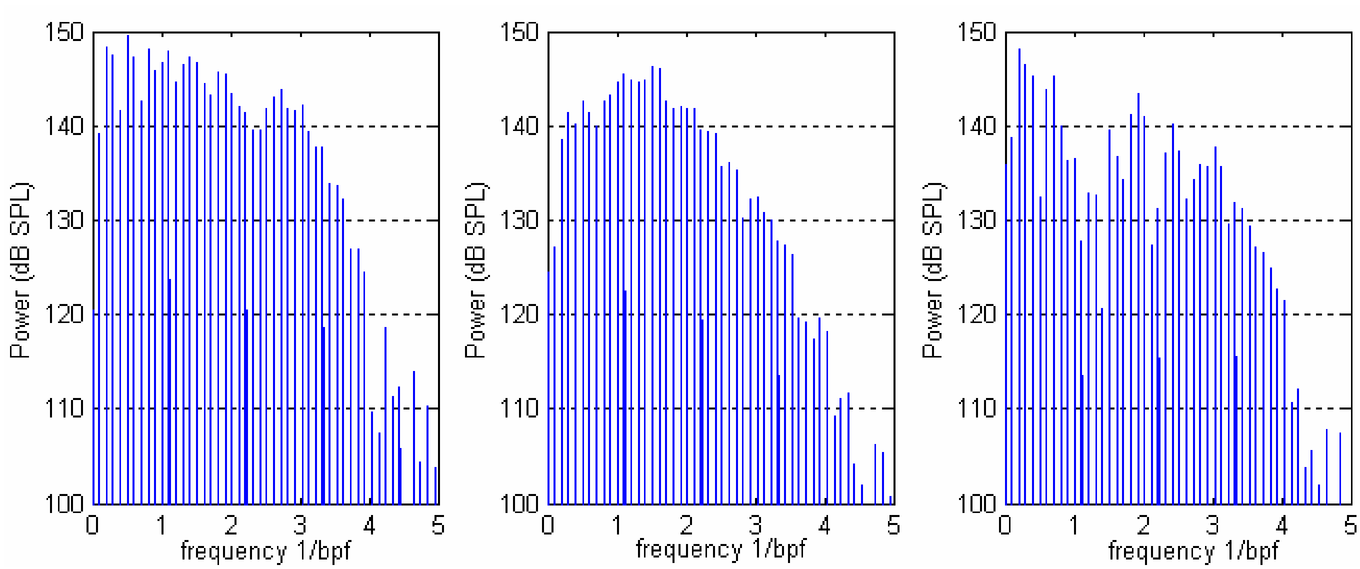

(a) Uncontrolled (b) Sinusoidal Articulation (c) Transient Articulation

Figure 17: Noise spectrum for uncontrolled (a) and two controlled cases (b,c).

is the convective delay past the stator. A positive disturbance δ_0' implies a late start and a negative disturbance an early start. For these experiments, t_c is 2.5 s.

The ΔOASPL is plotted in dB as a function of disturbances δ_0' in the control input timing (fig.18). These plots were created by using the same velocity fields shown in figures 15 and 16 and varying the time between the articulation start and

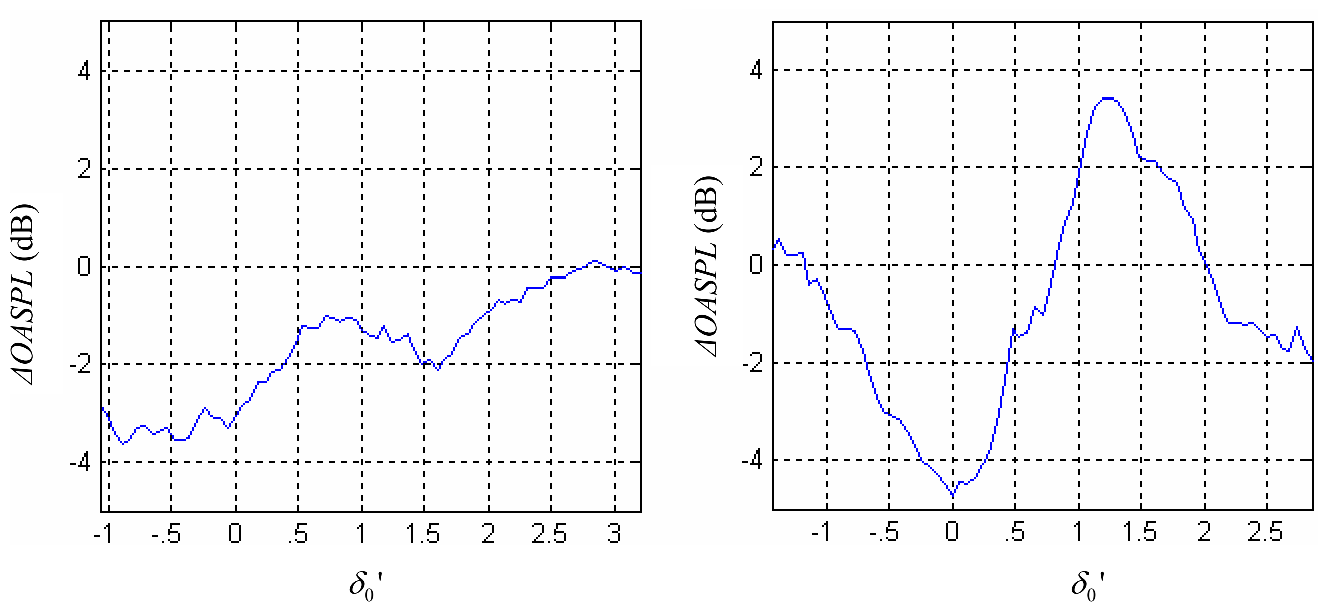

(a) Sinusoidal Articulation (b)Transient Articulation

Figure 18: Sensitivity of radiated noise to perturbations δ_0' in control start time.

the blade pass. Figures 18 (a) and (b) show that a zero δ_0' is optimal, which is obvious from the definition of δ_0' and t_0.

A continuous sinusoidal actuation (figs 10,15,17(b)) is naturally robust with regard to control synchronization, as shown in figure 18(a). As shown in figure 18(a), the effectiveness of a sinusoidal tail articulation mostly depends on having the control started sufficiently early. A control start timing disturbance of +2.5 is the threshold of no control effect. At that delay, the control input begins too late for flow modifications to convect downstream and affect noise generation. Start time disturbances in δ_0' in the range of 0 to 2.5 cause a blade pass during the startup transients of the tail motion, and start timing disturbances less than zero are during the steady state operation.

Transient tail motion (figs. 12,16,17(c)) appears to be most effective at noise reduction, but its unsteady nature makes this method susceptible to synchronization difficulties as shown in figure 18(b). Proper start timing (zero disturbance) can yield large reductions in radiated noise, but the control timing must be accurate. Timing disturbances between -0.5 and 0.5 in δ_0' allow effective noise reduction as the blade passes through the "gap" in the wake (figs. 12,16) created by the tail motion. However, disturbances of 0.8 to 2 in δ_0' actually cause an increase in noise. This implies that closed-loop control using unsteady force measurements on the blade could be quite useful for this application.

Before creating the "gap" in the wake deficit, the tail articulation causes a harmful wake disturbance visible at 14 seconds in figures 11 and 15. The additional noise production during disturbances of 0.8 to 2 in δ_0' occurs when the blade passes through this initial wake disturbance instead of the following "gap" in the wake.

7. SUMMARY AND CONCLUDING REMARKS

The flow around a stator with an articulated tail section was studied using a water tunnel and hot film anemometry in an attempt to reduce noise production. The tail articulation was provided by a conducting polymer (polypyrrole) actuator or by a stepper motor attached to an aluminum tail. The streamwise component of velocity was measured in time at different positions across the width of the tank.

A conducting polymer bilayer actuator was designed and fabricated to run in water. Its bandwidth and performance characteristics in water were tested. The polymer actuator shows the ability to alter the flow field for the tank speeds in this work (up to 6 cm/s). Using currently available CP technology, polymer actuators can only provide 40% of the required deflection at the minimum oscillation frequencies for wake deficit reduction.

The experimental results using a stepper motor showed that the wake deficit can be reduced by up to 60% with tail articulation. This reduction is most effective for Strouhal numbers from 0.25 to 0.35, the ideal efficient operating regime for efficient propulsion in fish [7]. A transient motion of the articulated tail provided the most effective wake deficit reduction, where the tail makes a relatively fast move and then settles.

Noise generation was predicted by passing a numerically simulated rotor blade through the measured flow field. Simulation shows that sound pressure level at dominant frequencies is reduced by 2-10 dB SPL using a constant sinusoidal tail motion, and by 2-25 dB using a transient tail motion.

The above results illustrate that tail articulation shows great promise for reducing noise production. If the tail articulation can be synchronized with the passing of a real rotor blade, large noise reductions (~6 dB OASPL) are possible. A simple sinusoidal tail oscillation also shows potential for noise reduction (~ 3dB OASPL).

Tail articulation appears most effective for the same Strouhal numbers as for propulsion efficiency in swimming fish. This is likely due to some form of thrust-inducing vortices that reduce the wake deficit. Transient tail motion is more effective than a constant oscillation due to startup transients.

Conducting polymer actuators are advancing rapidly and show promise. Though at the present time the CP-actuators can deliver 40% of the required performance capability for wake reduction, this relatively young technology is expected to bridge this gap in the near future.

Future work should include verifying these results on a larger model at faster speeds as this work is mainly a proof of concept. 3-D velocity measurements would allow study of the possibility of vortex formation as the underlying cause of the wake deficit reduction seen here.

Acknowledgements

This work is supported by the Office of Naval Research (N00014-02-1-0036), through the Biorobotics and Biomaterials program. We gratefully acknowledge the invaluable assistance of Professor Hunter, Director of Bioinstrumentation Laboratory, in the polymer growing and synthesis techniques which were central to the actuator development reported in this paper, Professor Ghoniem, MIT, and Dr. Raghu, Advanced Fluidics, in the interpretation of the flow field performance, and Dr. Annaswamy, in the overall research of active control of propulsor noise.

References

[1] P. R. Bandyopadhyay, "Maneuvering Hydrodynamics of Fish and Small Underwater Vehicles," *Journal of Integrative and Comparative Biology (formerly American Zoologist)*, vol. 42, No. 1, pp. 101-117, 2002.

[2] Bandyopadhyay, P. R., Krol, W. P., Thivierge, D. P., Nedderman, W. H. & Mojarrad, M. "A Biomimetic Propulsor for Active Noise Control: Experiments," NUWC TECH. REPT. 11,351, 2002. \

[3] P. R. Bandyopadhyay, J. M. Castano, J. Q. Rice, R. B. Philips, W. H. Nedderman, and W. K. Macy. "Low-Speed Maneuvering Hydrodynamics of Fish and Small Underwater Vehicles," *ASME Journal of Fluids Engineering*, vol. 119, 1997, pp. 136–144.

[4] F. E. Fish, "Performance Constraints on the Maneuverability of Flexible and Rigid Biological Systems," in *Proceedings of the 11th International Symposium on Unmanned Untethered Submersible Technology, Autonomous Undersea Systems Institute*, Durham, NH, 1999, pp. 394–406.

[5] F. E. Fish and J. Roh, "Review of Dolphin Hydrodynamics and Swimming Performance," Technical Report 1801, Space and Naval Warfare Systems Center, San Diego, CA, 1999.

[6] J. J. Rohr, E. W. Hendricks, L. Quigley, F. E. Fish, J. W. Gilpatrick, and J. Scardina-Ludwig, "Observations of Dolphin Swimming Speed and Strouhal Number," Technical Report 1769, Space and Naval Warfare Systems Center, San Diego, CA, 1998.

[7] M. Triantafyllou and G. Triantafyllou, "An Efficient Swimming Machine", *Scientific American*, vol. 272, March 1995, pp. 64–70.

[8] W.P Krol Jr., A.M. Annaswamy, P.R. Bandyopadhyay, "A Biomimetic Propulsor for Active Noise Control: Theory", *NUWC-NPT Technical Report 11,350*, 25 February 2002.

[9] J.D. Madden, R.A. Cush, T.S. Kanigan, I.W. Hunter, "Fast Contracting Polypyrrole Actuators", *Synthetic Metals* 113 (2000) 185-192.

[10] A. Della Santa, D. De Rossi, A. Mazzoldi, *Synthetic Metals* 90 (1997) 93-100.

[11] J.D. Madden, C.J. Brenan, J. Dubow, Progress Towards An Automatic, Microfabricated Polymer Air-Fluid Sampling Inlet, NTIS, Springfield, VA, 1997, Accession Number AS-A332 030/6/XAB.

[12] J.D. Madden, Conducting Polymer Actuators. In: *Ph.D. Thesis*, Department of Mechanical

Engineering, Massachusetts Institute of Technology, Cambridge, MA: 2000.

[13] J.D. Madden, R.A. Cush, T.S. Kanigan, C.J. Brennan, I.W. Hunter, *Synthetic Metals* 105 (1999) 61-64.

[14] Q. Pei, O. Inganas, *Solid State Ionics* 60 (1993) 161-166.

[15] R.H. Baughman, *Synthetic Metals* 78 (3) (1996) 339-353.

[16] A. Mazzoldi, A. Della Santa, D. De Rossi, in: Y. Osada, D.E. De Rossi (Eds.), *Polymer Sensors and Actuators*, Springer-Verlag, Heidelberg, 1999.

[17] M. Kaneko, M. Fukui, W. Takashima, K. Kaneto, *Synthetic Metals* 84 (1997) 795-796.

[18] Q. Pei, O. Inganas, "Conjugated polymers as smart materials, gas sensors and actuators using bending beams", *Synthetic Metals* 55–57 (1993) 247.

[19] J.M. Sansimena, V. Olazabal, T.F. Otero, C.N. daFonseca, M.A. DePaoli, A solid state artificial muscle based on polypyrrole and a solid polymeric electrolyte working in air, *Chemical Communication* 22 (1997) 2217.

[20] K. Kaneto, M. Kaneko, Y. Min, A.G. MacDiarmid, "Artificial muscle: electromechanical actuators using polyaniline films", *Synthetic Metals* 71 (1995) 2211.

[21] J.D. Madden, Progress Towards An Automatic, Microfabricated Polymer Air–Fluid Sampling Inlet, NTIS, Accession Number ADA332 030/6/XAB, Springfield, VA, 1997.

[22] M. Yamaura, K. Sato, K. Iwata, *Synthetic Metals* 48 (1992) 337-354.

[23] A. Noda, M. Watanabe, "Highly Conductive polymer electrodes prepared by insitu polymerization of vinyl monomers in room temperature molten salts", *Electrochimica Acta* 45 (2000) 1265-1270.

[24] B.S. Schmid, "Device Design and Mechanical Modeling of Conducting Polymer Actuators" Bachelors thesis, Department of Mechanical Engineering, Massachusetts Institute of Technology, Cambridge, MA: 2003.

[25] D.F. Opila, "Active Control of Underwater Propulsor Noise Using Polypyrrole Conducting Polymer Actuators" Masters thesis, Department of Mechanical Engineering, Massachusetts Institute of Technology, Cambridge, MA: 2003.

[26] D. Ross, *Mechanics of Underwater Noise*, Pergammon Press, Elmsford, NY, 1997